Experimental reconstruction of Wigner phase-space current

Yi-Ru Chen [ORCID],[1] Hsien-Yi Hsieh [ORCID],[1] Jingyu Ning,[1] Hsun-Chung Wu,[1] Hua Li Chen,[2] You-Lin Chuang,[3] Popo Yang,[1]
Ole Steuernagel,[1,4] Chien-Ming Wu,[1] and Ray-Kuang Lee [ORCID][1,2,3,5,*]

[1]*Institute of Photonics Technologies, National Tsing Hua University, Hsinchu 30013, Taiwan*
[2]*Department of Physics, National Tsing Hua University, Hsinchu 30013, Taiwan*
[3]*Physics Division, National Center for Theoretical Sciences, Taipei 10617, Taiwan*
[4]*Department of Physics, Astronomy and Mathematics, University of Hertfordshire, Hatfield, AL10 9AB, United Kingdom*
[5]*Center for Quantum Technology, Hsinchu 30013, Taiwan*

We experimentally reconstruct Wigner's current of quantum phase-space dynamics. We reveal the "push-and-pull" associated with damping and diffusion due to the coupling of a squeezed vacuum state to its environment. In contrast to classical dynamics, where (at zero temperature) dissipation only "pulls" the system toward the origin of phase space, we also observe an outward "push" because our system has to obey Heisenberg's uncertainty relations. With squeezed vacuum states generated by an optical parametric oscillator at variable pumping levels, we identify the pure squeezing dynamics and its central stagnation point with a topological charge of "−1". This work demonstrates high resolving power and establishes an experimental paradigm for measuring the quantumness and nonclassicality of the dynamics of open quantum systems.

I. INTRODUCTION

We establish experimentally that quantum dynamics in phase space can be studied directly and in great detail by using Wigner's quantum phase-space distribution W and the associated phase-space current $\vec{J}$ which governs W's time evolution. We do this in a quantum optical system using a degenerate squeezer setup.

Using Wigner's representation of quantum systems [1], based on Wigner's distribution $W(x, p)$ [2] in quantum phase space (with coordinates x for position and p for momentum), makes it easier to compare classical with quantum states than the commonly used density matrix ρ [3–6].

The Wigner distribution represents the quantum state, just like the density matrix; but the Wigner current describes the details of the quantum system dynamics, just like the commutator $[\hat{H}, \hat{\rho}]$. With the Wigner distribution, calculating other parameters such as fidelity, purity, and logarithmic negativity comes naturally, yet the Wigner current we reconstruct provides the most detailed way to extract the dynamics of the quantum system.

The associated Wigner current $\vec{J}$ allows for a direct visualization of the system dynamics and its comparison with classical Hamiltonian flows [7,8]. No such current exists to describe ρ's evolution (the commutator $[\hat{H}, \hat{\rho}]$ has not been studied by itself).

Any experimental quantum mechanical system is unavoidably subject to a number of dissipative processes, which, for our example, degrades squeezing, resulting in antisqueezing that is always larger than the squeezing. Losses and phase noise have to be taken into account to quantify this type of degradation of quantum states [9].

With the help of machine learning, our neural network-enhanced tomography has demonstrated good performance when extracting detailed information about the degradation in a system undergoing decoherence dynamics [10]. Here, we go one step further by reconstructing not only the Wigner distribution W, but also the associated Wigner current $\vec{J}$ experimentally. To access physically relevant structures in quantum phase space, our experimental reconstruction of the Wigner current allows identifying pure squeezing dynamics as well as dissipation and decoherence currents.

Dissipation drives the system toward the origin in phase space [11] by classical damping currents, as illustrated in Fig. 1. However, Heisenberg's uncertainty relation imposes a minimum phase-space area on the wave function, even for the (squeezed) vacuum state at zero temperature, prohibiting such purely classical dynamics. Here, we experimentally reveal the "push-and-pull" associated with this damping and diffusion due to the coupling of a squeezed vacuum state to its thermal environment.

The interplay of the corresponding contributions in the Wigner current $\vec{J}$ allows us to determine the phase-space currents, which, according to Eq. (5), describe absorption as well as spontaneous and induced emission processes. Since our system is measured in the steady state, this gives rise to detailed balance in a thermal background and therefore displays the phase-space current signatures associated with Einstein's A and B coefficients.

The remainder of this paper is organized as follows. In Sec. II we remind the reader of the connections between Wigner and Schrödinger representation of quantum theory, then, in Sec. III we illustrate the theoretical framework for

*rklee@ee.nthu.edu.tw

the Wigner current in our squeezer, including the damping and diffusive currents from the environment. Experimental reconstructions are demonstrated in Sec. IV, both for high and low purity conditions. Finally, we conclude in Sec. V.

II. WIGNER CURRENT $J(x, p, \tau)$ from Moyal's bracket

We first remind the reader of how Wigner's and Schrödinger's representations of quantum theory are connected mathematically [6]. Consider a single-mode operator given in coordinate representation $\langle x - y | \hat{O} | x + y \rangle = O(x - y, x + y)$. To map to Wigner's phase-space representation we employ the Wigner transform $\mathcal{W}[\hat{O}]$ [6,12,13],

$$\mathcal{W}[\hat{O}](x, p) = \int_{-\infty}^{\infty} dy \, O\left(x - \frac{y}{2}, x + \frac{y}{2}\right) e^{\frac{i}{\hbar} py}. \quad (1)$$

If $\hat{O}$ is a (normalized) single-mode density matrix $\hat{\rho}$, then the associated normalized distribution in the Wigner representation is $W(x, p) \equiv \mathcal{W}[\hat{\rho}]/(2\pi\hbar)$.

The Wigner transform of the von Neumann time evolution equation $\mathcal{W}[\frac{\partial \hat{\rho}}{\partial t} = \frac{1}{i\hbar}[\hat{H}(x, p, t), \hat{\rho}]]$ is

$$\frac{\partial W}{\partial t} = \{H(x, p, t), W\}, \quad (2)$$

in which the Groenewold-Moyal bracket [6,14,15] is the quantum version of the Poisson bracket [16], with the explicit form

$$\{f, g\} = \frac{2}{\hbar} f(x, p) \sin\left[\frac{\hbar}{2}\left(\frac{\overleftarrow{\partial}}{\partial x}\frac{\overrightarrow{\partial}}{\partial p} - \frac{\overleftarrow{\partial}}{\partial p}\frac{\overrightarrow{\partial}}{\partial x}\right)\right] g(x, p), \quad (3)$$

where the arrows indicate the "direction" of differentiation $f \overrightarrow{\frac{\partial}{\partial x}} g = g \overleftarrow{\frac{\partial}{\partial x}} f = f \frac{\partial}{\partial x} g$. Equation (2) can be rewritten as the divergence of Wigner's-phase space current [16,17], yielding the continuity equation

$$\frac{\partial W(x, p, t)}{\partial t} + \nabla \cdot \boldsymbol{J}(x, p, t) = 0. \quad (4)$$

Here, $\nabla = (\partial/\partial_x, \partial/\partial_p)$ is the divergence operator with respect to position x and momentum p, and t denotes time (but to be replaced by the effective time t_{eff} specified below), and $\boldsymbol{J} = (J_x, J_p)$ has two components and is a functional of W and the system Hamiltonian $H(x, p, t)$.

III. WIGNER CURRENT IN SQUEEZERS

After three decades of conceptual innovations and technological improvements [18,19] squeezed vacuum states [20–22], with up to 15-dB squeezing, were demonstrated [23]. To go beyond the standard quantum limit in measurements, squeezed vacuum states have been widely used in quantum metrology [24–27] and advanced gravitational wave detectors [28–34]. Here, we exploit the excellent control of such squeezer systems, which allows us to experimentally determine Wigner's distribution W and reconstruct Wigner's phase-space current $\vec{J} = (J_x, J_p)$ and its effects on the evolution of the system, with high resolution. Together, W and $\vec{J}$ fulfill the continuity equation (4).

Wigner's continuity equation (4) is the equivalent of the conventional von Neumann's equation. It was recently shown that it can be applied to open systems dynamics described by
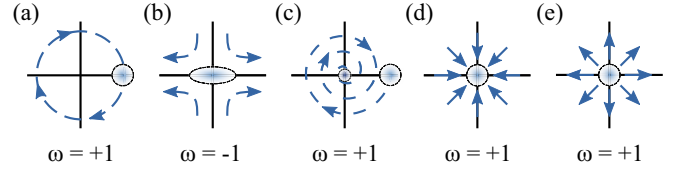

FIG. 1. Schematics of phase-space dynamics and the corresponding Wigner currents for (a) a coherent state, (b) a squeezed vacuum state (in a corotating frame), (c) the classical picture of a damped coherent state, (d) the damping current (with inward "pull"), and (e) the diffusing current (with outward "push"). ω is the winding number (9) of $\vec{J}$'s stagnation point at the origin.

standard Lindblad master equation terms [11,35] that describe the quantum dynamics of the open system state with the density matrix $\rho(t)$

$$\frac{d\rho}{dt} = -\frac{i}{\hbar}[H, \rho] + \frac{\gamma}{2}(\bar{n} + 1)(2a\rho a^\dagger - a^\dagger a\rho - \rho a^\dagger a)$$
$$+ \frac{\gamma}{2}\bar{n}(2a^\dagger \rho a - aa^\dagger \rho - \rho aa^\dagger). \quad (5)$$

Unlike this conventional approach, using Eq. (4) has the great advantage of allowing us to visualize quantum dynamics in phase space since W and $\vec{J}$ are real-valued. Indeed, the corresponding line integrals along $\vec{J}$ yield field lines, reminiscent of classical phase portraits [7,8].

Here we study squeezed vacuum states which can be produced by systems predominantly generating photon pairs, e.g., optical parametric oscillators (OPOs). In such degenerate processes, the effective Hamiltonian has the form [19–22]

$$\hat{H} = \frac{i\hbar \chi^{(2)}}{2}(\alpha^* \hat{a}^2 - \alpha \hat{a}^{\dagger 2}), \quad (6)$$

where α denotes the complex amplitude describing the pump field's strength and phase, while $\chi^{(2)}$ denotes the second-order nonlinear susceptibility. In Eq. (5), γ is the system energy damping rate and $\bar{n} = [\exp(\hbar\omega_0/k_B T) - 1]^{-1}$ accounts for the average environmental photon occupation number at the optical driving frequency ω_0 due to our experiment's effective thermal reservoir at temperature T.

The corresponding Wigner current of an ideal OPO system described by Eq. (6) driven at optical frequency ω_0, denoted as $\vec{J}_{\text{sys}}$, is illustrated in Fig. 1(b), and has the form

$$\vec{J}_{\text{sys}} = \chi^{(2)}|\alpha| \begin{pmatrix} x\, W \cos\theta + \frac{p}{\omega_0} W \sin\theta \\ \omega_0\, x\, W \sin\theta - p\, W \cos\theta \end{pmatrix} \quad (7)$$

$$= \xi \begin{pmatrix} \pm\frac{p}{\omega_0} W \\ \pm\omega_0\, x\, W \end{pmatrix} \quad \text{for} \quad \theta = \pm\pi/2, \quad (8)$$

with the squeezing parameter $\xi = \chi^{(2)}\alpha$.

Note, the Wigner current stagnation point at the origin of an OPO system has an orientation winding number topological charge of $\omega = -1$. This orientation winding number is defined as [7]

$$\omega[\mathcal{L}(x, p)] \equiv \frac{1}{2\pi} \oint_{\mathcal{L}(x, p)} d\phi, \quad (9)$$

and tracks the Wigner current's orientation along a simple closed-loop $\mathcal{L}$, i.e., around a single stagnation point (x, p), see Figs. 1 and Fig. 3.
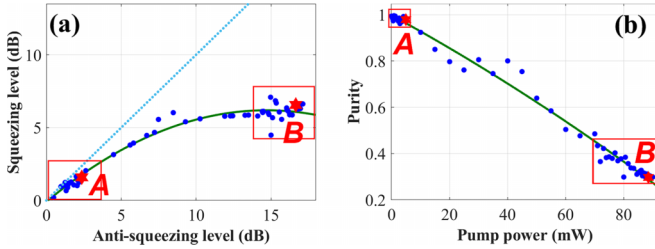
FIG. 2. (a) Measured quantum noise levels (in dB) of squeezing and antisqueezing quadratures at different pump powers. In the ideal case, squeezing and antisqueezing levels should be equal (blue dashed line). Because of losses and phase noise, due to coupling to the environment, we instead observe degraded squeezing performance described by the solid green fit line. (b) The corresponding purity $\text{tr}(\rho^2)$ of our squeezed states is determined using machine-learning enhanced quantum state tomography [10]. We highlight two regions with red boxes where the squeezing is "weak" and "strong." Specific red markers A and B pick out data points generated for "low" and "high" pump power, which are referred to in Fig. 3.

In open systems, damping processes occur due to the coupling to the environment and drive the initial wave package toward the origin. Figure 1(c) illustrates this for a damped classical harmonic oscillator. Note that, classically, the damping would concentrate the state ever more. In the quantum case, however, such a concentration would violate Heisenberg's uncertainty principle. Instead, our open dissipative system is well described by Eq. (5). The corresponding Wigner current $\vec{J}_{\text{env}}$ has a dissipative part $\vec{J}_{\text{damp}}$ and a diffusive part $\vec{J}_{\text{diff}}$, illustrated in Figs. 1(d) and 1(e), respectively, and of the form [11]

$$\vec{J}_{\text{env}} = -\frac{\gamma}{2} W \begin{pmatrix} x \\ p \end{pmatrix} - \frac{\gamma}{2} \frac{\hbar}{\omega_0} \left(\bar{n} + \frac{1}{2}\right) \begin{pmatrix} \partial_x W \\ \partial_p W \end{pmatrix} \qquad (10)$$

$$\equiv \vec{J}_{\text{damp}} + \vec{J}_{\text{diff}}. \qquad (11)$$

So far, all investigations of Wigner's current have been theoretical. Nevertheless, for slowly evolving systems, in general, it is almost always possible to identify and control an effective time τ_{eff} by changing a coupling constant in the Hamiltonian of the system; this is the approach we use. For an OPO Hamiltonian, $\hat{H}$, as in Eq. (6), the formal time evolution operator has the form

$$\hat{U}(\tau_{\text{eff}}) = \exp\left[\frac{-i\hat{H}\tau_{\text{eff}}}{\hbar}\right] = \exp\left[\frac{\chi^{(2)}}{2}(\alpha^*\hat{a}^2 - \alpha\hat{a}^{\dagger 2})\right], \qquad (12)$$

of a squeezing transformation $\hat{S}(\xi) = \exp[\frac{1}{2}(\xi^*\hat{a}^2 - \xi\hat{a}^{\dagger 2})]$. This allows us to connect our experimental parameters with the effective time parameter $\tau_{\text{eff}} \propto |\xi| = \chi^{(2)}|\alpha|$ in continuity equation (4). In other words, varying the pump power amounts to a formal variation of the evolution time and allows us to utilize the Wigner current $\vec{J}$ of Eq. (4), also see Appendix A.

IV. EXPERIMENTS

Here, we generate squeezed vacuum states in a bow-tie OPO cavity enclosing a periodically poled nonlinear KTiOPO$_4$ (PPKTP) crystal with second-order nonlinear susceptibility $\chi^{(2)}$, operating below the lasing threshold at the wavelength 1064 nm [10]. Such a bow-tie cavity can compensate for the intracavity dispersion [36].

Our cavity has an optical path length of approximately 28.5 cm and thus a free spectral range of 1.052 GHz, with finesse of 19.8 at 532 nm and of 33.4 at 1064 nm. The overall efficiency, defined as $1 - L$ (the loss), is $82.2 \pm 0.35\%$ and phase noise is 34.50 ± 1.26 mrad.

By injecting the ac signal of our balanced homodyne detection, the spectrum analyzer records the squeezing and antisqueezing levels when scanning the phase of the local oscillator. In Fig. 2(a), we show the measured noise-level curves for squeezing and antisqueezing in decibel (dB) while the pump power increases from 0 to 90 mW. The magnitude of squeezing and antisqueezing levels are almost the same at low pump power levels, indicating that the generated squeezed states are almost pure. However, degradation arises due to the coupling to the environment, giving roughly 7.08 dB in squeezing but 14.97 dB in antisqueezing at 76 mW. When the experiments are performed with pump power at 5 mW, each photodiode of our balanced homodyne detector is illuminated with 15 mW. The (electronic) dark noise level is -87.69 dB, while the vacuum noise level is -64.34 dB, giving a shot-noise level of 23.35 dB. The measurement is done with the spectrum analyzer at 2.5 MHz with 100 001 data points, 100-kHz resolution bandwidth, and 100-Hz video bandwidth. To make sure the measured squeezing level is not contaminated, our homodyne detectors are designed with a high common-mode rejection ratio of more than 80 dB [37].

We use machine learning to perform quantum state tomography experimentally, after that a singular value decomposition of the reconstructed density matrix gives three dominant terms

$$\rho \approx \sigma_1\,\rho^{\text{sq}} + c_1\,\rho_{\text{th}}^{\text{sq}} + d_1\,\rho_{\text{th}}. \qquad (13)$$

Here, ρ^{sq} denotes the (pure) squeezed vacuum, $\rho^{\text{sq}} = \hat{S}\rho_0\hat{S}^{\dagger}$, with ρ_0 the vacuum state and S given by Eq. (12). Due to coupling to the environment, the two dominant admixtures are from thermal states ρ_{th} and squeezed thermal states $\rho_{\text{th}}^{\text{sq}} = \hat{S}\rho_{\text{th}}\hat{S}^{\dagger}$ [38–41]. As shown in Fig. 2(b), the corresponding purity $\text{tr}(\rho^2)$ of measured squeezed states decreases as the pump power increases.

To reconstruct Wigner's current we increase the pump power by 20 discrete steps of 0.25 mW each. This translates into effective time steps times $\tau_j \propto |\alpha_j|$ which allows us to approximate $\partial W_{\text{exp}}(x, p)/\partial \tau_{\text{eff}}$ in the continuity equation (4).

The corresponding Wigner current $\vec{J}_{\text{exp}}$ is then reconstructed using the parameters for the state given in Eq. (13), which, in turn, give us the effective weights with which we weigh the respective contributions from ideal system current $\vec{J}_{\text{sys}}$ in Eq. (7) and the environmental current $\vec{J}_{\text{env}}$ in Eq. (10). (For details see Appendix A).

In Figs. 3(a) to 3(c), we observe that the experimentally reconstructed currents $\vec{J}_{\text{exp}}$ for squeezed vacuum states follow hyperbolic curves aligned with the squeezed and antisqueezed quadratures. Compared to the pure-system current $\vec{J}_{\text{sys}}$ predicted by theory in Eq. (8), shown in Figs. 3(d) to 3(f), the experimentally observed current $\vec{J}_{\text{exp}}$, displayed in Figs. 3(a) to 3(c), shows modifications due to decoherence processes:
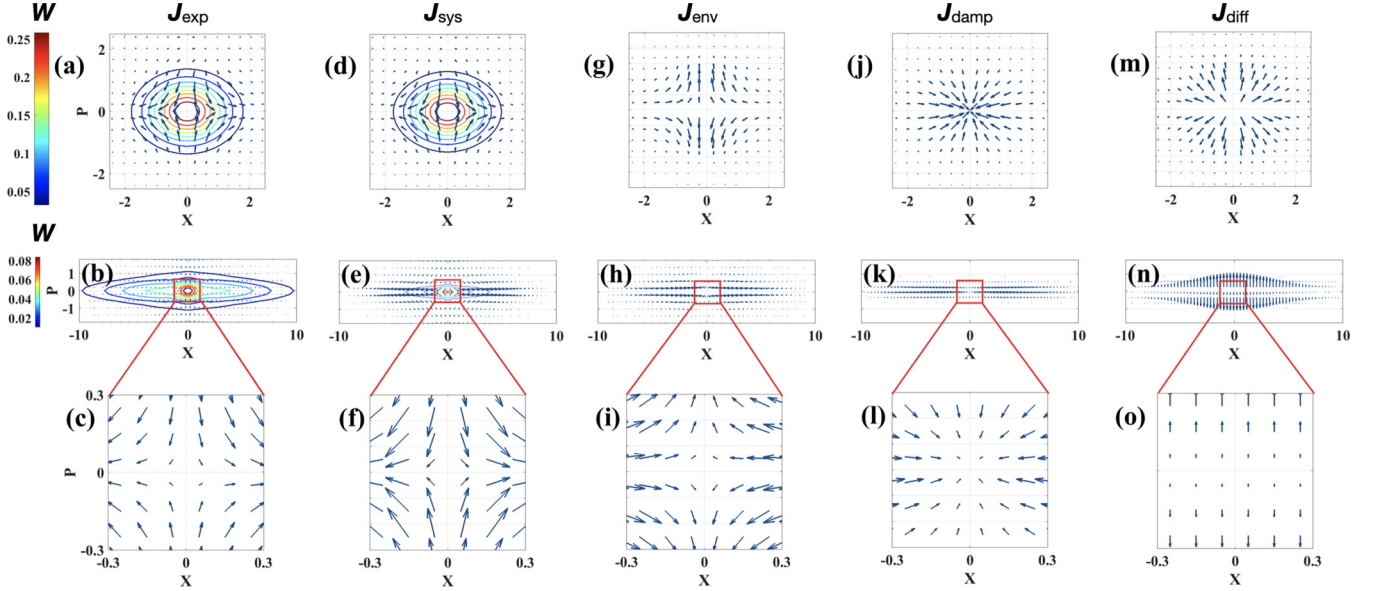
FIG. 3. Top and middle rows: Snapshots of Wigner current distributions, displayed as blue arrows (in arbitrary units), overlaid over colored contours of the corresponding Wigner distributions of squeezed vacuum states. The top row represents a weakly squeezed state generated at an OPO pump power of 4.75 mW and selected by marker *A* in Fig. 2. Similarly, the middle row represents a strongly squeezed state at 88 mW pump power, selected by marker *B*. The Wigner current displays, circumscribed by red boxes in the middle row, are shown magnified in the bottom row. They illustrate how, even for strong coupling to the environment, the topological charge $\omega(0, 0)$ of $\vec{J}_{\text{sys}}$ is preserved. First column (a)–(c) : Wigner current $\vec{J}_{\text{exp}}$, reconstructed from experimental data. Second column (d)–(f): the ideal Wigner current $\vec{J}_{\text{sys}}$, fitted to pure squeezed states. Third column (g)–(i): Thermal contributions in the Wigner current $\vec{J}_{\text{env}} = \vec{J}_{\text{exp}} - \vec{J}_{\text{sys}}$, extracted from the experimental data (by subtraction of the second column from the first column data). Fourth column (j)–(l): Dissipative part of Wigner current $\vec{J}_{\text{damp}}$ in Eq. (10). Fifth column (m, n): Diffusive part of Wigner current $\vec{J}_{\text{diff}}$ in Eq. (10). Note that adding $\vec{J}_{\text{damp}}$ and $\vec{J}_{\text{diff}}$ in the fourth and fifth columns, respectively, yields $\vec{J}_{\text{env}}$ shown in the third column: $\vec{J}_{\text{env}} = \vec{J}_{\text{damp}} + \vec{J}_{\text{diff}}$. We emphasize that, to make them clearly comparable with $\vec{J}_{\text{exp}}$ and $\vec{J}_{\text{sys}}$ in (a, d), we had to increase the magnitudes of $\vec{J}_{\text{env}}$, $\vec{J}_{\text{damp}}$, and $\vec{J}_{\text{diff}}$ in (g), (j), and (m) by scale factors 375, 125, and 125, respectively.

expansions of the Wigner distributions and some distortions in the currents. Their difference $\vec{J}_{\text{env}} = \vec{J}_{\text{exp}} - \vec{J}_{\text{sys}}$ is displayed in the third columns of Figs. 3(g) to 3(i). It graphically displays how the system's current is locally counteracted by the currents due to the coupling to the environment.

A. Low power, weak squeezing (*P* = 4.75 mW)

To analyze and deepen our understanding of the roles played by the environment currents further, let us use Eq. (10) to decompose the Wigner distribution current $\vec{J}_{\text{env}}$ into the dissipative $\vec{J}_{\text{damp}}$ and diffusive part $\vec{J}_{\text{diff}}$, see the fourth and fifth columns of Fig. 3. Here, the experimentally determined Wigner function W_{exp} is used to generate the dissipative and diffusive currents, $\vec{J}_{\text{damp}}$ and $\vec{J}_{\text{diff}}$, employing the two fitting parameters $\gamma = 0.01$ and $\bar{n} = 0.1$. These were extracted from the respective three weights in Eq. (13) which change little as the pump power is increased to a low power of 5 mW, see Fig. 2. This confirms that our system is stable since losses due to the environment are fairly constant. This squeezer system is exquisitely controllable and thus "clean" enough to allow us to emphasize what conceptual clarity and experimental resolving power our toolbox of Wigner current measurements provides.

We find $\vec{J}_{\text{diff}}$ in Eq. (10) is dominated by the quantum vacuum contribution $\vec{J}_{\text{diff}} \approx -\frac{\gamma}{2} \frac{\hbar}{\omega_0} \frac{1}{2} (\partial_x W, \partial_p W)^{\text{T}}$, as sketched in Fig. 1(e). We emphasize that, to make them clearly comparable with $\vec{J}_{\text{exp}}$ and $\vec{J}_{\text{sys}}$ in Figs. 3(a) and 3(d), we had to

increase the magnitudes of $\vec{J}_{\text{env}}$, $\vec{J}_{\text{damp}}$, and $\vec{J}_{\text{diff}}$ in Figs. 3(g), 3(j) and 3(m) by scale factors 375, 125, and 125, respectively. This demonstrates the impressive control over our system and sensitivity to details of the dynamics and thus the strength of our approach (for more details see Appendix B).

B. High power, strong squeezing (*P* = 88 mW)

In our system, strong pumping, leading to strong squeezing simultaneously increases coupling to the environment and thus a pronounced reduction in the state's purity, see Fig. 2(b). The more squeezed the state, the less it shows rotational symmetry in phase space, as can be seen clearly in Fig. 3(b).

Yet, irrespective of the strength of the coupling to the environment, the environment's influence does not change the origin stagnation point's topological charge $\omega[\mathcal{L}(0, 0)] = -1$.

That this charge remains constant even in the case of strongly driven, strongly dissipative systems can be understood as the OPO squeezer supplying the primary driving force, against which the environment reacts with dissipation and diffusion. Since the environment "reacts," it only "compensates" but cannot "overcome" the OPO's driving to impose a dynamic with entirely different topological characteristics. It thus reduces the effect of the OPO's driving without fundamentally altering the origin's charge of $\omega = -1$.

Note that in the second row of Fig. 3 the scale factor shown is 1, indicating the low purity of the squeezed states. We want

to remark that $\vec{J}_{\mathrm{diff}}$ is state dependent [but $\vec{J}_{\mathrm{damp}}$ is not, see Figs. 3(k) and 3(l) as well as Eq. (10)], this strongly modifies the diffusive Wigner current, see Figs. 3(n) and 3(o). Together they form the overall environmental Wigner current shown in Figs. 3(h) and 3(i), which is counteracting the system's squeezing action. In terms of the underlying physical mechanisms we interpret our results as a *push-and-pull* scenario playing out in front of our eyes:

The squeezer-system current $\vec{J}_{\mathrm{sys}}$ "pushes" the state along the x axis while the environmental current $\vec{J}_{\mathrm{env}}$ counteracts by "pulling backwards." $\vec{J}_{\mathrm{env}}$, in turn, should be interpreted as the interplay between damping due to emission, see the fourth column of Fig. 3 [and also Fig. 1(d)], and quantum diffusion due to absorption, see fifth column of Fig. 3 [and Fig. 1(e)]. In the steady state, these processes give rise to the Einstein coefficients. Here we display their associated phase-space signatures.

V. CONCLUSION

With the help of machine-learning-enhanced quantum state tomography, we experimentally reconstruct the Wigner distribution and its phase-space current of squeezed vacuum states through the one-to-one mapping between the pump power and an effective time parameter. We find a Wigner current stagnation point at the origin and confirmed its orientation winding number topological charge as $\omega = -1$ and that it is constant [7]. The analysis of the Wigner current due to interactions with the thermal environment reveals a push-and-pull between its damping and diffusive parts.

In addition to the squeezed states investigated here, our methodology can be readily applied to other families of quantum states, such as single-photon states, "cat" states, and quantum-optical engineering states [42–45], for the studies on their evolution and interactions with outside systems. Moreover, with recent theoretical developments in systems described by anharmonic Hamiltonians [46,47], effectively non-Hermitian parity-time symmetric Hamiltonians [48] and even in discrete (spin) systems [49,50], our experimental implementation promises to provide us with a powerful diagnostic toolbox.

APPENDIX A: WIGNER CURRENT RECONSTRUCTION

Here, we illustrate how to reconstruct $\vec{J}_{\mathrm{exp}}$. Under the slowly varying pumping power condition, we need to find δJ_x and δJ_p. We do this by minimizing their 1-norm

$$\underset{\delta J_x, \delta J_p}{\mathrm{minimize}} \left|\left| \begin{bmatrix} \delta J_x \\ \delta J_p \end{bmatrix} \right|\right|_1, \tag{A1}$$

subject to the continuity equation

$$\frac{\partial}{\partial t} W + \frac{\partial}{\partial x}\left(J_x^{\mathrm{initial}} + \delta J_x\right) + \frac{\partial}{\partial p}\left(J_p^{\mathrm{initial}} + \delta J_p\right) = 0. \tag{A2}$$

Here, J_x^{initial} and J_p^{initial} are assigned as the initial guesses.

Equivalently, we treat this as an optimization problem, taking the continuity equation as an equality constraint. Then, by using machine-learning-enhanced quantum state tomography [10], we reconstruct the density matrix, as well as the corresponding $W(x, p, \tau_{\mathrm{eff}})$, from the experimental data at different effective times. To avoid nonphysical states, we impose on the reconstructed density matrix the constraint to be positive-semi-definite. To achieve this we use an auxiliary lower triangle matrix generated by a Cholesky decomposition which generates the density matrix. Once we determined the Wigner distribution, the Wigner current is automatically defined with the help of a given Hamiltonian, see Eq. (4).

Explicitly, we treat δJ_x and δJ_p as the variables and solve the set of equations

$$D_x \, \delta J_x + D_p \, \delta J_p = \frac{W_t - W_{t+1}}{\Delta t} - D_x \, J_x^{\mathrm{initial}} - D_p \, J_p^{\mathrm{initial}}. \tag{A3}$$

Here, the unknown variables are $\delta J_x \in R^{n^2 \times 1}$ and $\delta J_p \in R^{n^2 \times 1}$, with n being the grid number in both x and p coordinates. To perform the calculations on a discrete version of the continuity equation, we also applied differential operators (forward finite difference), i.e., the differential matrices D_x and D_p shown in Eq. (A3). Finally, this 1-norm minimization problem can be transformed into a standard linear programming problem by using reformulation techniques [51].

APPENDIX B: RECONSTRUCTED CURRENTS AT LOW POWER: HIGH RESOLVING POWER OF OUR APPROACH

For very moderate squeezing, information about the degradation of the purity $\mathrm{tr}(\rho^2)$ of the quantum state in our squeezing setup is shown in Fig. 2(b) as a function of the pump power. The purity of our squeezed vacuum remains as high as ≈ 0.98, even working at 5-mW pump power. Yet unavoidable decoherence from the interaction with the environment is in evidence. Its effects on the Wigner current are shown in Fig. 4, which displays a series of experimentally determined snapshots of the Wigner current $\vec{J}_{\mathrm{exp}}$ as the pump power is increased; the colored contours of the corresponding Wigner distributions are shown in the background.

In the first columns in Figs. 4(a) to 4(d) the Wigner current $\vec{J}_{\mathrm{exp}}$ is reconstructed from the experimental data at OPO pump powers 0.25, 1.75, 3.25, and 4.75 mW, respectively. The second columns in Figs 4(e) to 4(h) show the ideal Wigner current $\vec{J}_{\mathrm{sys}}$ fitted to pure squeezed states. The third columns in Figs. 4(i) to 4(l) demonstrate the thermal contributions in the Wigner current $\vec{J}_{\mathrm{env}} = \vec{J}_{\mathrm{exp}} - \vec{J}_{\mathrm{sys}}$, extracted from the experimental data (by subtraction of the second column from the first column data). The fourth column is Figs. 4(m) to 4(p) are the dissipative parts of the Wigner current, $\vec{J}_{\mathrm{damp}}$ in Eq. (10). The fiifth columns in Figs. 4(q) to 4(t) represent the diffusion parts of the Wigner current, $\vec{J}_{\mathrm{diff}}$ in Eq. (10).
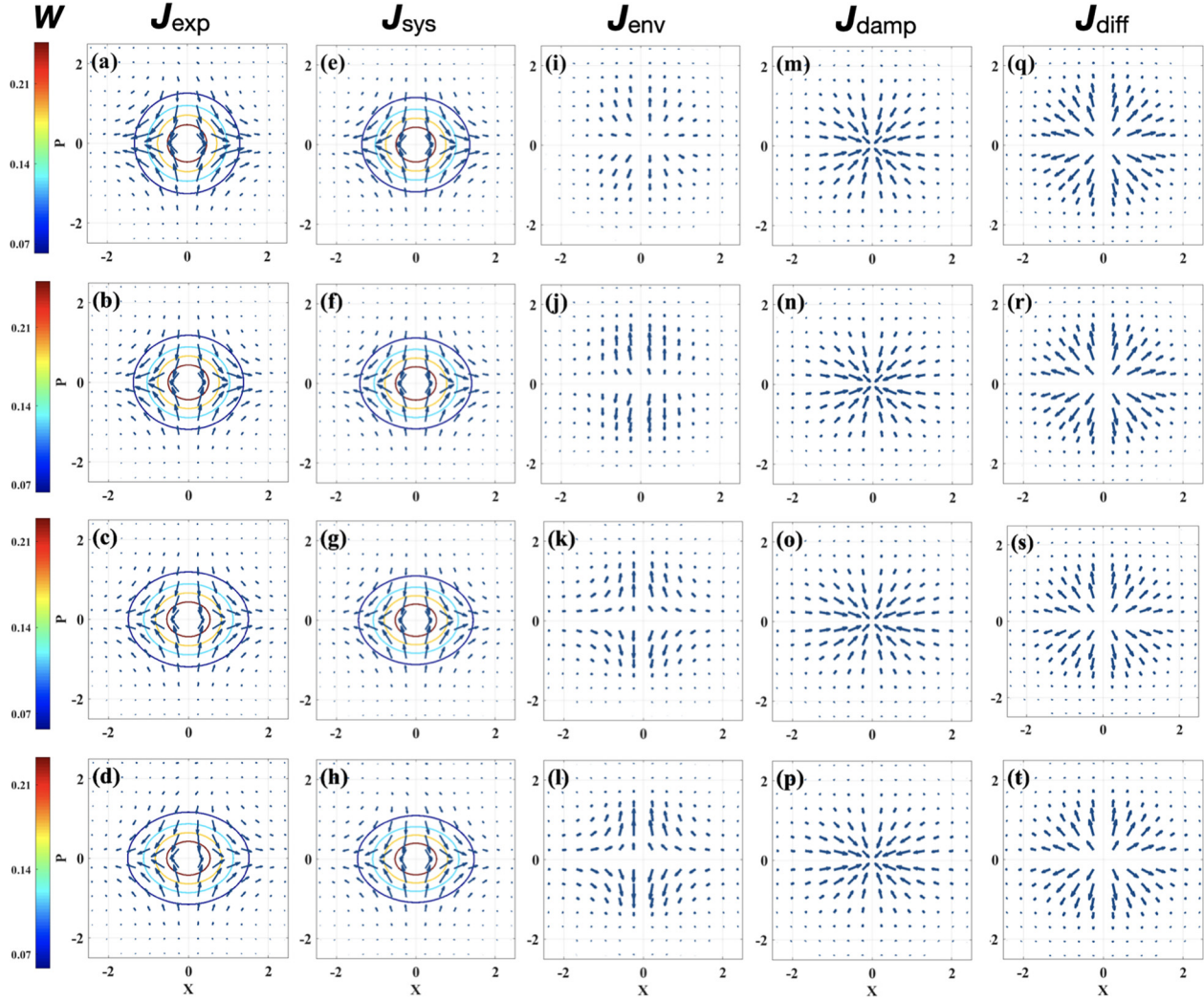
FIG. 4. Snapshots of Wigner current distributions (arrows, displayed in arbitrary units) of squeezed vacuum states at moderate squeezing, with the colored contours of corresponding Wigner distributions shown in the background. From top to bottom, the corresponding OPO pump powers are 0.25, 1.75, 3.25, and 4.75 mW. From left to right shows the experimental Wigner current $\vec{J}_{\mathrm{exp}}$, the ideal Wigner Current $\vec{J}_{\mathrm{sys}}$, the environmental current $\vec{J}_{\mathrm{env}} = \vec{J}_{\mathrm{exp}} - \vec{J}_{\mathrm{sys}}$, the damping current $\vec{J}_{\mathrm{damp}}$, and the diffusive current $\vec{J}_{\mathrm{diff}}$, respectively. Note that we also have $\vec{J}_{\mathrm{env}} = \vec{J}_{\mathrm{damp}} + \vec{J}_{\mathrm{diff}}$.

(Note that adding $\vec{J}_{\mathrm{damp}}$ and $\vec{J}_{\mathrm{diff}}$ in the fourth and ffth columns, respectively, yields $\vec{J}_{\mathrm{env}}$ shown in the third column, i.e., $\vec{J}_{\mathrm{env}} = \vec{J}_{\mathrm{damp}} + \vec{J}_{\mathrm{diff}}$.)

We emphasize that to make them clearly comparable with $\vec{J}_{\mathrm{exp}}$ and $\vec{J}_{\mathrm{sys}}$ in Fig. 4 (columns "1" and "2"), we had to

increase the magnitudes of $\vec{J}_{\mathrm{env}}$, $\vec{J}_{\mathrm{damp}}$, and $\vec{J}_{\mathrm{diff}}$ in Fig. 4, columns "3," "4," and "5," by scale factors 375, 125, and 125, respectively. This demonstrates the impressive control over our system and sensitivity to details of the dynamics and thus the strength of our approach

[1] E. Wigner, On the quantum correction for thermodynamic equilibrium, Phys. Rev. **40**, 749 (1932).

[2] A. Royer, Wigner function as the expectation value of a parity operator, Phys. Rev. A **15**, 449 (1977).

[3] U. Leonhardt and H. Paul, Measuring the quantum state of light, Prog. Quantum Electron. **19**, 89 (1995).

[4] W. P. Schleich, *Quantum Optics in Phase Space* (Wiley-VCH, Weinheim, Germany, 2001).

[5] W. H. Zurek, Sub-planck structure in phase space and its relevance for quantum decoherence, Nature (London) **412**, 712 (2001).

[6] T. L Curtright, D. B Fairlie, and C. K. Zachos, *A Concise Treatise on Quantum Mechanics in Phase Space* (World Scientific, Singapore, 2014).

[7] O. Steuernagel, D. Kakofengitis, and G. Ritter, Wigner Flow Reveals Topological Order in Quantum Phase Space Dynamics, Phys. Rev. Lett. **110**, 030401 (2013).

[8] D. Kakofengitis and O. Steuernagel, Wigner's quantum phase-space current in weakly-anharmonic weakly-excited two-state systems, Eur. Phys. J. Plus **132**, 381 (2017).

[9] L. McCuller *et al.*, Ligos quantum response to squeezed states, Phys. Rev. D **104**, 062006 (2021).

[10] H.-Y. Hsieh, Y.-R. Chen, H.-C. Wu, H. L. Chen, J. Ning, Y.-C. Huang, C.-M. Wu, and R.-K. Lee, Extract the Degradation Information in Squeezed States with Machine Learning, Phys. Rev. Lett. **128**, 073604 (2022).

[11] W. F. Braasch, O. D. Friedman, A. J. Rimberg, and M. P. Blencowe, Wigner current for open quantum systems, Phys. Rev. A **100**, 012124 (2019).

[12] J. Hancock, M. A. Walton, and B. Wynder, Quantum mechanics another way, Eur. J. Phys. **25**, 525 (2004).

[13] D. Cohen, Lecture notes in quantum mechanics, arXiv:quant-ph/0605180.

[14] H. J. Groenewold, On the principles of elementary quantum mechanics, Physica **12**, 405 (1946).

[15] J. E. Moyal, Quantum mechanics as a statistical theory, Proc. Cambridge Philos. Soc. **45**, 99 (1949).

[16] M. Oliva, D. Kakofengitis, and O. Steuernagel, Anharmonic quantum mechanical systems do not feature phase space trajectories, Physica A **502**, 201 (2018).

[17] M. Oliva and O. Steuernagel, Quantum kerr oscillators' evolution in phase space: Wigner current, symmetries, shear suppression and special states, Phys. Rev. A **99**, 032104 (2019).

[18] R. E. Slusher, L. W. Hollberg, B. Yurke, J. C. Mertz, and J. F. Valley, Observation of Squeezed States Generated by Four-Wave Mixing in an Optical Cavity, Phys. Rev. Lett. **55**, 2409 (1985).

[19] L.-A. Wu, H. J. Kimble, J. L. Hall, and H. Wu, Generation of Squeezed States by Parametric Down Conversion, Phys. Rev. Lett. **57**, 2520 (1986).

[20] H. P. Yuen, Two-photon coherent states of the radiation field, Phys. Rev. A **13**, 2226 (1976).

[21] D. F. Walls and G. J. Milburn, *Quantum Optics*, 2nd ed. (Springer, New York, 1984).

[22] U. L. Andersen, T. Gehring, C. Marquardt, and G. Leuchs, 30 years of squeezed light generation, Phys. Scr. **91**, 053001 (2016).

[23] H. Vahlbruch, M. Mehmet, K. Danzmann, and R. Schnabel, Detection of 15 dB Squeezed States of Light and their Application for the Absolute Calibration of Photoelectric Quantum Efficiency, Phys. Rev. Lett. **117**, 110801 (2016).

[24] D. J. Wineland, J. J. Bollinger, W. M. Itano, F. L. Moore, and D. J. Heinzen, Spin squeezing and reduced quantum noise in spectroscopy, Phys. Rev. A **46**, R6797(R) (1992).

[25] V. Giovannetti, S. Lloyd, and L. Maccone, Quantum-enhanced measurements: beating the standard quantum limit, Science **306**, 1330 (2004).

[26] V. Giovannetti, S. Lloyd, and L. Maccone, Advances in quantum metrology, Nat. Photonics **5**, 222 (2011).

[27] S. Steinlechner, J. Bauchrowitz, M. Meinders, H. Muller-Ebhardt, K. Danzmann, and R. Schnabel, Quantum-dense metrology, Nat. Photonics **7**, 626 (2013).

[28] C. M. Caves, Quantum-mechanical noise in an interferometer, Phys. Rev. D **23**, 1693 (1981).

[29] H. Grote, K. Danzmann, K. L. Dooley, R. Schnabel, J. Slutsky, and H. Vahlbruch, First Long-Term Application of Squeezed States of Light in a Gravitational-Wave Observatory, Phys. Rev. Lett. **110**, 181101 (2013).

[30] L. Barsotti, J. Harms, and R. Schnabel, Squeezed vacuum states of light for gravitational wave detectors, Rep. Prog. Phys. **82**, 016905 (2019).

[31] M. Tse *et al.*, Quantum-Enhanced Advanced LIGO Detectors in the Era of Gravitational-Wave Astronomy, Phys. Rev. Lett. **123**, 231107 (2019).

[32] F. Acernese *et al.* (Virgo Collaboration), Increasing the Astrophysical Reach of the Advanced Virgo Detector via the Application of Squeezed Vacuum States of Light, Phys. Rev. Lett. **123**, 231108 (2019).

[33] Y. Zhao, N. Aritomi, E. Capocasa, M. Leonardi, M. Eisenmann, Y. Guo, E. Polini, A. Tomura, K. Arai, Y. Aso *et al.*, Frequency-Dependent Squeezed Vacuum Source for Broadband Quantum Noise Reduction in Advanced Gravitational-Wave Detectors, Phys. Rev. Lett. **124**, 171101 (2020).

[34] L. McCuller, C. Whittle, D. Ganapathy, K. Komori, M. Tse, A. Fernandez-Galiana, L. Barsotti, P. Fritschel, M. MacInnis, F. Matichard, K. Mason, N. Mavalvala, R. Mittleman, H. Yu, M. E. Zucker, and M. Evans, Frequency-Dependent Squeezing for Advanced LIGO, Phys. Rev. Lett. **124**, 171102 (2020).

[35] R. Cabrera, Denys I. Bondar, K. Jacobs, and H. A. Rabitz, Efficient method to generate time evolution of the wigner function for open quantum systems, Phys. Rev. A **92**, 042122 (2015).

[36] S. S. Y. Chua, M. S. Stefszky, C. M. Mow-Lowry, B. C. Buchler, S. Dwyer, D. A. Shaddock, P. K. Lam, and D. E. McClelland, Backscatter tolerant squeezed light source for advanced gravitational-wave detectors, Opt. Lett. **36**, 4680 (2011).

[37] C.-M. Wu, S.-R. Wu, Y.-R. Chen, H.-C. Wu, and R.-K. Lee, Detection of 10 db vacuum noise squeezing at 1064 nm by balanced homodyne detectors with a common mode rejection ratio more than 80 db, in *Conference on Lasers and Electro-Optics*, edited by Osa Technical (Optica, Washington, DC, 2019), p. JTu2A–38.

[38] G. S. Agarwal, Wigner-function description of quantum noise in interferometers, J. Mod. Opt. **34**, 909 (1987).

[39] S. Chaturvedi and V. Srinivasan, Photon-number distributions for fields with Gaussian wigner functions, Phys. Rev. A **40**, 6095 (1989).

[40] N. Lütkenhaus and S. M. Barnett, Nonclassical effects in phase space, Phys. Rev. A **51**, 3340 (1995).

[41] H.-C. Yuan and X.-X. Xu, Squeezed vacuum state in lossy channel as a squeezed thermal state, Mod. Phys. Lett. B **29**, 1550219 (2015).

[42] A. Ourjoumtsev, R. Tualle-Brouri, J. Laurat, and P. Grangier, Generating optical schrödinger kittens for quantum information processing, Science **312**, 83 (2006).

[43] H. Takahashi, K. Wakui, S. Suzuki, M. Takeoka, K. Hayasaka, A. Furusawa, and M. Sasaki, Generation of Large-Amplitude Coherent-State Superposition via Ancilla-Assisted Photon Subtraction, Phys. Rev. Lett. **101**, 233605 (2008).

[44] D. V. Sychev, A. E. Ulanov, A. A. Pushkina, M. W. Richards, I. A. Fedorov, and A. I. Lvovsky, Enlargement of optical schrödinger's cat states, Nat. Photonics **11**, 379 (2017).

[45] E. Bimbard, N. Jain, A. MacRae, and A. I. Lvovsky, Quantum-optical state engineering up to the two-photon level, Nat. Photonics **4**, 243 (2010).

[46] R. T. Skodje, H. W. Rohrs, and J. VanBuskirk, Flux analysis, the correspondence principle, and the structure of quantum phase space, Phys. Rev. A **40**, 2894 (1989).

[47] M. Oliva and O. Steuernagel, Dynamic Shear Suppression in Quantum Phase Space, Phys. Rev. Lett. **122**, 020401 (2019).

[48] L. Praxmeyer, P. Yang, and R.-K. Lee, Phase-space representation of a non-hermitian system with pt symmetry, Phys. Rev. A **93**, 042122 (2016).

[49] P. Yang, I. F. Valtierra, A. B. Klimov, S.-T. Wu, R.-K. Lee, L. L. Sánchez-Soto, and G. Leuchs, The wigner flow on the sphere, Phys. Scr. **94**, 044001 (2019).

[50] I. F. Valtierra, A. B. Klimov, G. Leuchs, and L. L. Sanchez-Soto, Quasiprobability currents on the sphere, Phys. Rev. A **101**, 033803 (2020).

[51] J. Nocedal and S. J. Wright, *Numerical Optimization* (Springer, New York, 1999).